Combined effect of annealing temperature and vanadium substitution for mangetocaloric $Mn_{1.2-x}V_xFe_{0.75}P_{0.5}Si_{0.5}$ alloys

Lai, Jiawei; Huang, Bowei; Miao, Xuefei; Van Thang, Nguyen; You, Xinmin; Maschek, Michael; van Eijck, Lambert; Zeng, Dechang; van Dijk, Niels; Brück, Ekkes

DOI
10.1016/j.jallcom.2019.06.239

Publication date
2019

Document Version
Final published version

Published in
Journal of Alloys and Compounds

Journal of Alloys and Compounds 803 (2019) 671–677

Contents lists available at ScienceDirect

Journal of Alloys and Compounds

journal homepage: http://www.elsevier.com/locate/jalcom

Combined effect of annealing temperature and vanadium substitution for mangetocaloric $Mn_{1.2-x}V_xFe_{0.75}P_{0.5}Si_{0.5}$ alloys

Jiawei Lai [a, b, *], Bowei Huang [a, b], Xuefei Miao [b, e], Nguyen Van Thang [b, d], Xinmin You [b], Michael Maschek [b], Lambert van Eijck [c], Dechang Zeng [a, **], Niels van Dijk [b], Ekkes Brück [b]

[a] School of Materials Science & Engineering, South China University of Technology, Guangzhou, 510640, China
[b] Fundamental Aspects of Materials and Energy, Department of Radiation Science and Technology, Delft University of Technology, Mekelweg 15, 2629JB, Delft, the Netherlands
[c] Neutron and Positron Methods in Materials, Department of Radiation Science and Technology, Delft University of Technology, Mekelweg 15, 2629 JB, Delft, the Netherlands
[d] Department of Chemistry, Quy Nhon University, 170 An Duong Vuong, QuyNhon, BinhDinh, Viet Nam
[e] Jiangsu Key Laboratory of Advanced Micro & Nano Materials and Technology, School of Materials Science and Engineering, Nanjing University of Science and Technology, Nanjing, 210094, China

ARTICLE INFO

Article history:
Received 4 March 2019
Received in revised form
12 June 2019
Accepted 18 June 2019
Available online 20 June 2019

Keywords:
$(Mn, V, Fe)_{1.95}(P, Si)$
Neutron diffraction
Magnetocaloric
Magnetic properties
Entropy

ABSTRACT

Approaching the border of the first order transition and second order transition is significant to optimize the giant magnetocaloric materials performance. The influence of vanadium substitution in the $Mn_{1.2-x}V_xFe_{0.75}P_{0.5}Si_{0.5}$ alloys is investigated for annealing temperatures of 1323, 1373 and 1423 K. By tuning both the annealing temperature and the V substitution simultaneously, the magnetocaloric effect can be enhanced without enlarging the thermal hysteresis near the border of the first to second order transition. Neutron diffraction measurements reveal the changes of site occupation and interatomic distances caused by varying the annealing temperature and V substitution. The properties of the alloy with $x = 0.02$ annealed at 1323 K is comparable to those found for the $MnFe_{0.95}P_{0.595}Si_{0.33}B_{0.075}$ alloy, illustrating that $Mn_{1.2-x}V_xFe_{0.75}P_{0.5}Si_{0.5}$ alloys are excellent materials for magnetic heat-pumping near room temperature.

1. Introduction

Recently, near room temperature magnetic heat-pumping technology has attracted broad attention due to its high efficiency, low impact on the environment, low noise, and long service life compared with the conventional vapor-compression technology [1]. The giant magnetocaloric effect (GMCE) materials, which are utilized as active regenerator, form a key factor to determine the efficiency of this technology. GMCE occurs in some materials that undergo a first-order magnetic transition (FOMT), such as $Gd_5Ge_2Si_2$ [2], $LaFe_{13-x}Si_x$ [3–5], $MnFeP_{1-x-y}Si_xB_y$ [6–8], $MnCoGeB_x$ [9] and Heusler [10] alloys. Among them, the $MnFeP_{1-x-y}Si_xB_y$ alloys are currently regarded as one of the most promising materials that can be industrialized because of their cheap and non-toxic elements, high cooling capacity and tunable T_C near room temperature [7]. Nevertheless, thermal hysteresis (ΔT_{hys}) in $MnFeP_{1-x-y}Si_x$ alloys still limits their application since it lowers the efficiency of the cooling cycle. Lots of research has been done to reduce ΔT_{hys} while maintaining the GMCE. In order to obtain a limited ΔT_{hys}, the compositions can be tuned to shift the FOMT towards the border with a second-order magnetic phase transition (SOMT), as demonstrated for $MnFeP_{1-x-y}Si_xB_y$ [11] or for the transition metal substitution in $Mn_{1-y}Co_yFe_{0.95}P_{0.50}Si_{0.50}$ and $MnFe_{0.95-x}Ni_xP_{0.50}Si_{0.50}$ [12]. Additionally, ΔT_{hys} can also be controlled by the annealing time and temperature. For example, in $Mn_{1.15}Fe_{0.85}P_{0.55}Si_{0.45}$ alloys [13], ΔT_{hys} decreases with the annealing temperature. The effect of the annealing temperature and time on the magnetic phase transition of $Mn_{1.000}Fe_{0.950}P_{0.595}Si_{0.330}B_{0.075}$ alloys have been investigated [14] and the annealing temperature was found to show a strong influence on ΔT_{hys}. $Mn_{1.2}Fe_{0.75}P_{0.5}Si_{0.5}$ alloys [15] annealed at 1373 K in a two-step heat treatment process were reported to have a strong FOMT with a relatively low ΔT_{hys} of 5 K.

However, the combined effect of the annealing temperature and

* Corresponding author. School of Materials Science & Engineering, South China University of Technology, Guangzhou, 510640, China.
** Corresponding author.
E-mail address: scutjiaway@gmail.com (J. Lai).

https://doi.org/10.1016/j.jallcom.2019.06.239
0925-8388/

element substitutions has not been studied yet. Sintering of Mn-Fe-P-Si alloys can be regarded as a solid-state diffusion process as the annealing temperature is below the melting point (1553 K). The diffusion rate of each element strongly dependents on the annealing temperature. Therefore, introducing extra elements in the Mn-Fe-P-Si alloy requires a different annealing temperature. Here we report the combined effect of a changing annealing temperature (1323, 1373 and 1423 K) and V substitution ($x = 0.00, 0.01, 0.02, 0.03, 0.04, 0.05$) in $Mn_{1.2-x}V_xFe_{0.75}P_{0.5}Si_{0.5}$ alloys, resulting in a change in the hexagonal crystal structure and the magnetic properties. The substitution of Mn by V can be controlled by adjusting the annealing temperature in order to approach the border of the FOMT and SOMT.

2. Experimental

Polycrystalline $Mn_{1.2-x}V_xFe_{0.75}P_{0.5}Si_{0.5}$ ($x = 0.00, 0.01, 0.02, 0.03, 0.04, 0.05$) alloys were prepared by powder metallurgy. The starting materials Mn (99.7%), Fe (99.7%), red P (99%), Si (99.7%) and V (99.5%) powders were mechanically ball milled in a PULVERRISETTE 5 planetary mill for 10 h in an Ar atmosphere with a constant rotation speed of 380 rpm, then pressed into small tablets (ø 13 mm, mass 3–5 g), and finally sealed in quartz ampoules under 200 mbar of Ar. These tablets were then annealed at 1323, 1373 and 1423 K for 2 h in order to promote crystallization and slowly cooled down to room temperature. Subsequently, they were heated up to the same annealing temperature for 20 h to homogenize and quenched in water.

The X-ray diffraction (XRD) patterns were collected on a PANalytical X-pert Pro diffractometer with Cu-Kα radiation (1.54056 Å) at room temperature (RT). The room-temperature neutron diffraction data were collected at a wavelength of 1.67105 Å on the neutron powder diffraction instrument PEARL [16] at the research reactor of Delft University of Technology. The crystal structures and atom occupancies were refined using the Rietveld refinement method implemented in the Fullprof software package [17,18]. The temperature and magnetic field dependence of the magnetization was measured by a superconducting quantum interference device (SQUID) magnetometer (Quantum Design MPMS 5XL) in the reciprocating sample option (RSO) mode. The adiabatic temperature change (ΔT_{ad}) is measured in a Peltier cell based DSC using a Halbach cylinder magnetic field ($\leq$1.5 T). In this setup, the iso-field calorimetric scans were performed at a rate of 3.0 K/min, while the temperature lag due to the thermal resistance of the Peltier cells has been corrected.

3. Results and discussions

The magnetization as a function of the temperature for $Mn_{1.2-x}V_xFe_{0.75}P_{0.5}Si_{0.5}$ ($x = 0.00, 0.01, 0.02, 0.03, 0.04$ and 0.05) alloys after annealing at 1323, 1373 and 1423 K is shown in Fig. 1. The values are extracted from iso-field measurements (decreasing from 2 to 0.2 T in steps of 0.2 T) to ensure that thermal history effects are removed. The ferromagnetic - to - paramagnetic transition temperature T_C is determined by the corresponding temperature where a maximum is observed in the $|dM/dT|$ curves. T_C tends to decrease with increasing V substitution after annealing at 1323, 1373 and 1423 K, as shown in Fig. 1 (*d*). For the alloys annealed at 1373 K, T_C deviates from the linearity in the $x = 0.02$, in which the sample shows a higher low field MCE, see Fig. 4 (b). T_C is sensitive to

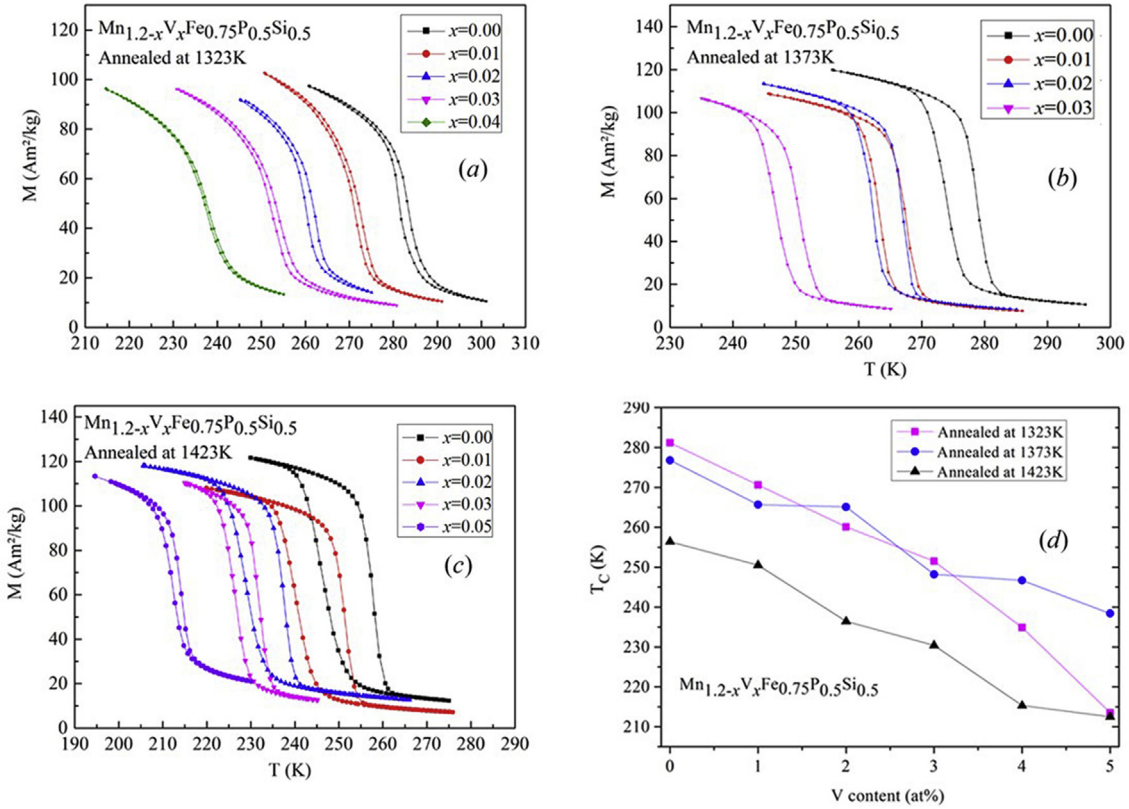

Fig. 1. Magnetizations as a function of temperature for $Mn_{1.2-x}V_xFe_{0.75}P_{0.5}Si_{0.5}$ ($x = 0.00, 0.01, 0.02, 0.03, 0.04$ and 0.05) alloys after annealing at (*a*) 1323 K, (*b*) 1373 K and (*c*) 1423 K; (*d*) The T_C for $Mn_{1.2-x}V_xFe_{0.75}P_{0.5}Si_{0.5}$ alloys after annealing at 1323, 1373, 1423 K.

changes in internal structure or internal symmetry [19]. The observed changes are in good agreement with the trends for the *c/a* ratio in the refined lattice parameters (see Fig. 2(*d*)).

The thermal hysteresis ΔT_{hys} is defined as the difference in T_C for the heating and cooling process, which will hinder the efficiency of the magnetic cooling [20]. It is important to minimize ΔT_{hys} while maintaining a sufficient GMCE. In this work, ΔT_{hys} is determined by the difference in the transition temperature during heating and cooling in a field of 1 T. The values of T_C, ΔT_{hys} and latent heat (L) for the $Mn_{1.2-x}V_xFe_{0.75}P_{0.5}Si_{0.5}$ ($x = 0.00$, 0.01, 0.02, 0.03, 0.04, 0.05) alloys after annealing at 1323, 1373 and 1423 K are shown in Table 1. Since materials with a pronounced FOMT usually show large L values [21], the values of L can be regarded as a sign of the strength of the FOMT. In general, V substitutions for Mn can reduce both ΔT_{hys} and L. When x increases from 0.00 to 0.05, ΔT_{hys} decreases dramatically from 12.8 K to 1.4 K for annealing at 1423 K, while it decrease from 2.1 K to below the experimental resolution for annealing at 1323 K. Note that the limited ΔT_{hys} for the $Mn_{1.2-x}V_xFe_{0.75}P_{0.5}Si_{0.5}$ alloys annealed at 1323 K is promising for practical applications. For the alloy with $x = 0.02$ the values of ΔT_{hys} and L are unexpectedly larger than those for $x = 0.01$ for annealing at 1323 and 1373 K, which suggests a stronger first-order transition. As shown in Table 2, the increase in occupation of Fe on the 3*f* site may contribute to a strengthened FOMT.

Rietveld refinement of room-temperature XRD data shows that, in the $Mn_{1.2-x}V_xFe_{0.75}P_{0.5}Si_{0.5}$ alloys, the hexagonal Fe_2P-type phase (space group P-*62 m*) corresponds to the main phase and a $MnFe_2Si$-type phase (space group F*m3m*) is found as impurity phase [22]. The impurity phase fraction for each annealing temperature (see Fig. 2) is roughly at the same level for $x \leq 0.04$, which allows for an independent comparison of the effects of V substitution on the alloys annealed at the same annealing temperature. For the alloys with $x \leq 0.03$ annealed at 1323 and 1373 K, the impurity phase fraction is around 8.0 ± 1.0 vol%. When the annealing temperature rises to 1423 K, the impurity increases to around 11.5 ± 0.5 vol%. These results indicate that a large impurity phase-fraction will be introduced at a higher annealing temperature. The higher fraction of impurity can be one of the reasons for the

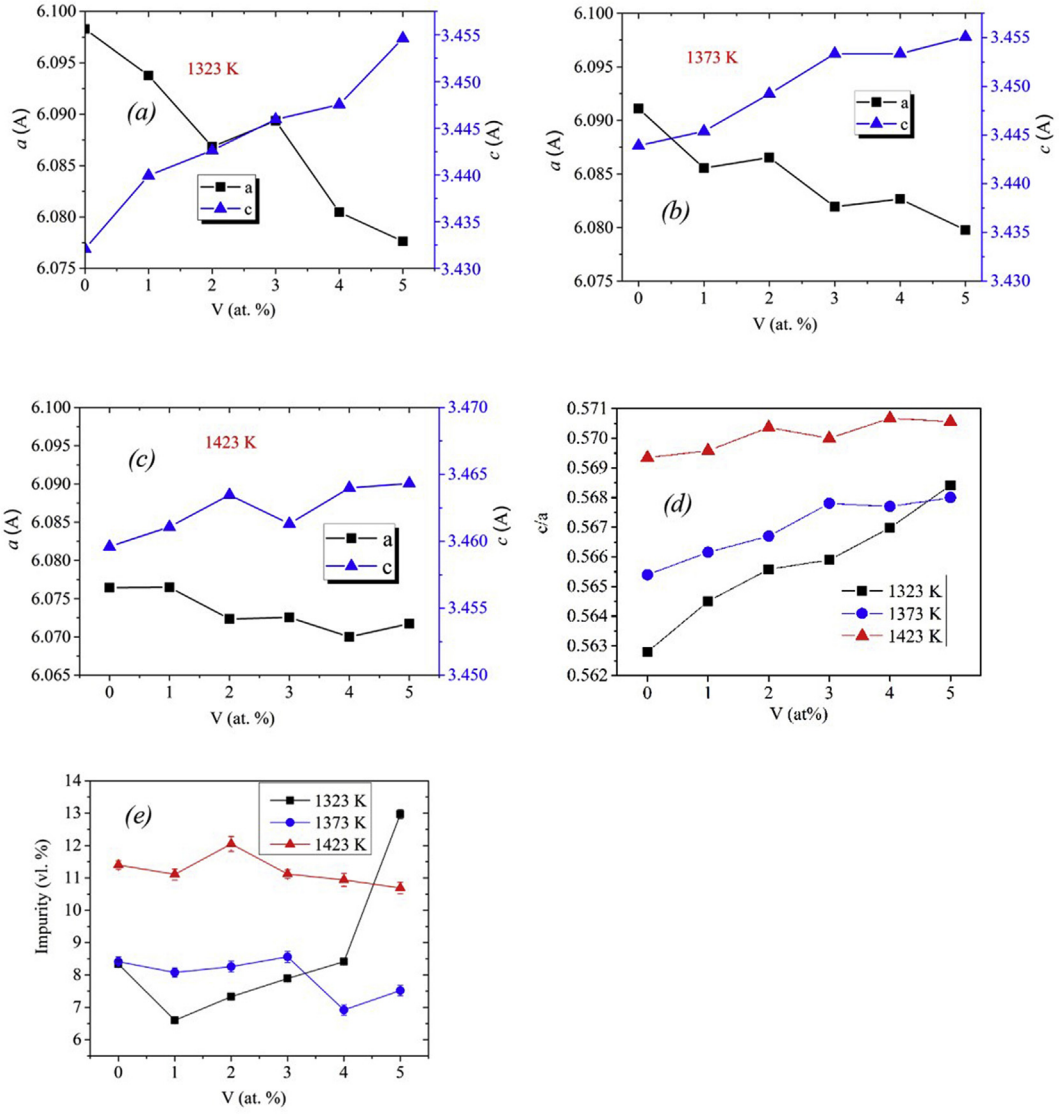

Fig. 2. Relationship between the (*a*–*c*) lattice parameters *a* and *c*, (*d*) *c/a*, and (*e*) the phase fraction of impurity phase and the V content of $Mn_{1.2-x}V_xFe_{0.75}P_{0.5}Si_{0.5}$ ($x = 0.00$, 0.01, 0.02, 0.03, 0.04, 0.05) alloys after annealing at 1323, 1373 and 1423 K.

Table 1
Values of T_C, ΔT_{hys} and the latent heat (L) for $Mn_{1.2-x}V_xFe_{0.75}P_{0.5}Si_{0.5}$ ($x = 0.00, 0.01, 0.02, 0.03, 0.04, 0.05$) alloys after annealing at 1323, 1373 and 1423 K, respectively.

x	Annealed at 1423 K			Annealed at 1373 K			Annealed at 1323 K		
	T_C (K)	ΔT_{hys} (K)	L (kJ/kg)	T_C (K)	ΔT_{hys} (K)	L (kJ/kg)	T_C (K)	ΔT_{hys} (K)	L (kJ/kg)
0.00	256.4	12.8	7.6	276.8	4.5	8.0	281.2	2.1	6.2
0.01	250.5	10.7	7.1	265.7	3.5	7.6	270.6	1.3	4.8
0.02	236.4	9.1	5.9	265.1	4.7	8.4	260.1	1.8	4.2
0.03	230.4	5.4	5.6	248.2	3.7	6.3	251.5	1.3	3.9
0.04	215.3	3.8	4.5	246.7	–	5.5	234.9	1.0	3.3
0.05	212.5	1.4	3.5	238.4	–	4.9	213.5	–	0.04

Table 2
The site occupation of the 3*f*, 3*g*, and 2*c* sites for the $Mn_{1.2}Fe_{0.75}P_{0.5}Si_{0.5}$ alloys annealed at 1323, 1373 and 1423 K and the $Mn_{1.18}V_{0.02}Fe_{0.75}P_{0.5}Si_{0.5}$ alloy annealed at 1373 K. Space group: *P*-62 *m*. Atomic positions: 3*f* (x_1,0,0), 3*g* (x_2,0,1/2), 2*c* (1/3,2/3,0), and 1*b* (0,0,1/2).

Site	Parameters	$x = 0.00$ 1323 K	$x = 0.00$ 1373 K	$x = 0.00$ 1423 K	$x = 0.02$ 1373 K
3*f*	*a*	6.107(4)	6.098(2)	6.082(3)	6.093(1)
	c	3.427(7)	3.442(4)	3.460(6)	3.448(8)
	V(Å^3)	110.723(9)	110.858(8)	110.897(11)	110.884(8)
	x_1	0.2536(4)	0.2539(4)	0.2528(5)	0.2542(4)
	n(Fe)/*n*(Mn)	0.193/0.057(4)	0.200/0.050(5)	0.203/0.047(7)	0.183/0.065(4)
	n(V)	0.00	0.00	0.00	0.005(4)
3*g*	x_2	0.5924(7)	0.5921(7)	0.5927(8)	0.5923(7)
	n(Mn)/*n*(Fe)	0.25/0.00	0.25/0.00	0.25/0.00	0.25/0.00
2*c*	*n*(P)/*n*(Si)	0.093/0.074(3)	0.107/0.060(3)	0.097/0.070(4)	0.083/0.084(4)
1*b*	*n*(P)/*n*(Si)	0.032/0.052(3)	0.019/0.065(3)	0.028/0.055(4)	0.042/0.041(4)
	Rp(%)	6.46	6.62	7.32	7.47
	wRp(%)	8.95	8.89	10.1	9.66
	χ^2	7.53	6.63	12.1	5.71

larger ΔT_{hys} as was proposed by Gutfleisch et al. [23].

From crystal structure refinement (summarized in Fig. 2), we observe trends for the lattice parameter change as a function of V concentration, which are similar for all the three annealing temperatures: the *a* axis decreases and the *c* axis increases, leading to an increase in *c*/*a* ratio. The deviation of lattice parameters from linearity is related to the fluctuation of impurity since the 3:1 phase of impurity affects the metallic and non-metallic ratio in the Fe_2P-type, see Fig. 2 (e). The amplitude of the change varies according to the annealing temperature. For $x = 0.05$, the change in *c*/*a* ratio is 1.0, 0.5 and 0.4% at an annealing temperature of 1323, 1373 and 1423 K, respectively. There is a smaller change at higher annealing temperatures, which may be caused by some segregation into the inter-grain secondary phase, as can be seen in Fig. 2 (*e*).

In the Mn-rich Mn-Fe-P-Si alloy, it is reported that the Fe atoms preferentially occupy the 3*f* site, the Mn atoms the 3*g* site, the P atoms and Si atoms the 2*c* or 1*b* sites randomly [24]. X-ray absorption and powder diffraction experiments combined with density functional theory (DFT) calculations revealed that an electronic redistribution takes place in Mn-Fe-P-Si-B, which is at the origin of the giant entropy change and results in a large change in the electron density for Fe on the 3*f* site and the surrounding Si/P atoms. [25].

Additionally, first-principles calculations suggest that larger magnetic moments will develop on the *3f* and *3g* sites when there are more coplanar Si nearest neighbors [26]. In order to investigate the relationship between the site occupancies and the magneto-elastic phase transition, it is significant to investigate both the atom positions and the site occupation in the Fe_2P-type structure. As shown in Table 2, the P and Si atoms occupy the *2c* and *1b* site randomly and the *3g* site is fully occupied by Mn, which is consistent with a previous study [25]. Note that, the occupation of Fe on the *3f* site increases when the annealing temperature increases.

Fig. 3 (*a*) shows the neutron diffraction pattern and the refinement of the $Mn_{1.18}V_{0.02}Fe_{0.75}P_{0.5}Si_{0.5}$ alloy annealed at 1373 K. To investigate the site preference for V in the Fe_2P-type structure, refinements have been conducted assuming that V is (i) all located exclusively on the 3*f* site, (ii) located exclusively on the 3*g* site or (iii) randomly distributed over the 3*f* and 3*g* sites, resulting in χ^2 values of 5.16, 16.4 and 5.19, respectively. From these results it is concluded that V has a slight preference to occupy the 3*f* site.

For the alloys annealed at 1373 K, the sample with $x = 0.02$ has a higher $|\Delta S_M|$ value for a field change of 1 T than the sample with $x = 0$ (see Fig. 4(b)). This is probably due to an enhanced magnetic coupling caused by V on the 3*f* site (shown in Table 2). Fig. 3 (*b*) shows the lattice parameters calculated from the neutron diffraction patterns, which are consistent with results from XRD patterns. The *a*-axis decreases and the *c*-axis increases when increasing the annealing temperature. The sample with $x = 0.02$ has a smaller *a*-axis and a larger *c*-axis compared to the one without V.

In the Fe_2P-type structure, the magneto-elastic coupling originates from so called mixed magnetism: the Mn/Fe (3*f*)-P/Si (2*c*) hybridizing in the same plane ($z = 0$) undergoes a meta-magnetic transition, while the Mn (3*g*)-P/Si (1*b*) in the other plane ($z = 0.5$) have large stable moments [27]. The development of the Fe moment (3*f*) is in strong competition with the formation of chemical bonds, which depends on the intra-atomic distances between Fe and its neighbors. The size of the Mn moment on the 3 g site is less influenced by the intra-atomic distances, which reflects the localized character. [28] Fig. 3 (*c*) and (*d*) illustrates the interatomic distance as a function of annealing temperature for $Mn_{1.2}Fe_{0.75}P_{0.5}Si_{0.5}$ alloys and the open symbols represent the $Mn_{1.18}V_{0.02}Fe_{0.75}P_{0.5}Si_{0.5}$ annealed at 1373 K. The interatomic distances are listed in Table 3. When increasing the annealing temperature of $Mn_{1.2}Fe_{0.75}P_{0.5}Si_{0.5}$ alloy, the mean intra-layer distance Mn/Fe(3*f*)-P/Si (2*c*) increases while the intra-layer distance Mn/Fe(3*f*)-Mn/Fe (3*f*) decreases. This will increase the chemical bonding and lead to a decrease in transition temperature. The mean intra-layer distance Mn(3*g*)-P/Si (1*b*) decreases (Fig. 3(*d*)), while the layer of Mn(3*g*)-Mn(3*g*) decrease(Fig. 3(*c*)). The mean distance

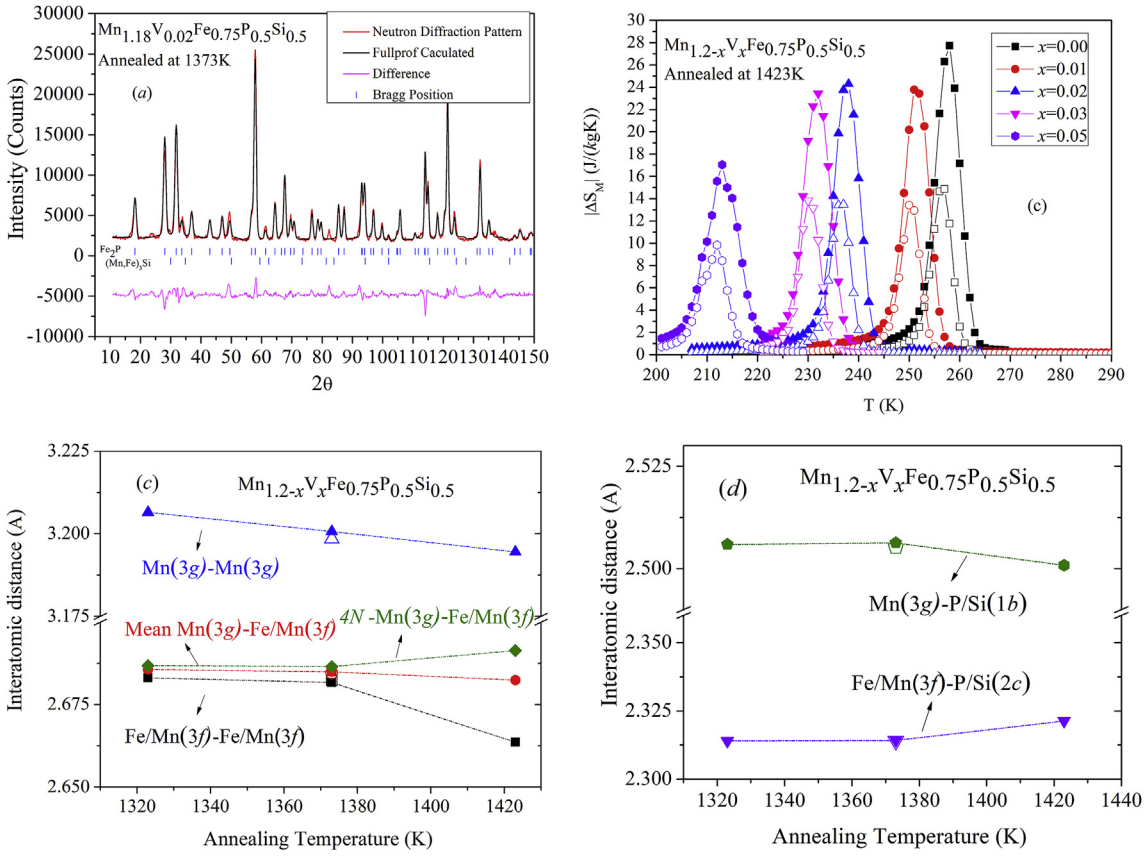

Fig. 3. (*a*) Neutron diffraction patterns and the refinement result of the $Mn_{1.18}V_{0.02}Fe_{0.75}P_{0.5}Si_{0.5}$ alloy annealed at 1373 K; (*b*), (*c*) and (*d*) lattice parameters and interatomic distance as a function of annealing temperature for the $Mn_{1.2}Fe_{0.75}P_{0.5}Si_{0.5}$ alloys and the open symbols represent the data for the $Mn_{1.18}V_{0.02}Fe_{0.75}P_{0.5}Si_{0.5}$ annealing at 1373 K.

of interlayer Mn (3*g*) - Mn/Fe (3*f*) has no notable change when increasing the annealing temperature. However, the distance of interlayer Mn (3*g*)-Mn/Fe (3*f*) that has 4 bonds in neighbor (the diamond symbols) increases, shown in Fig. 3 (*c*). These competitions weakens the magnetic exchange interaction in the Mn(3*g*) site and results in a decrease in the transition temperature T_C. Compared to the alloy without V annealed at 1373 K, the $Mn_{1.18}V_{0.02}Fe_{0.75}P_{0.5}Si_{0.5}$ alloy annealed at 1373 K, indicating as the open symbols in Fig. 3(*c*) and (*d*), also has slightly smaller mean distance of both the intra layer Mn (3*g*)-P/Si (1*b*) and Mn (3*g*)-Mn (3*g*). This shrinkage in the plane ($z = 0.5$) can explain the decreases in T_C induced by the V substitution.

The iso-field magnetization curves of annealed $Mn_{1.2-x}V_xFe_{0.75}P_{0.5}Si_{0.5}$ ($x = 0.00, 0.01, 0.02, 0.03, 0.04, 0.05$) for a magnetic field change of 0–2 T are measured in the vicinity of T_C at temperature intervals of 1 K. The $|\Delta S_M|$ values of the alloys is derived from extracted isothermal magnetization curves based on the Maxwell relation [29,30].

Temperature dependence of $|\Delta S_M|$ for a field change of 0–1 T (open symbols) and 0–2 T (solid symbols) for $Mn_{1.2-x}V_xFe_{0.75}P_{0.5}Si_{0.5}$ ($x = 0.00$, 0.01, 0.02, 0.03, 0.04, and 0.05) alloys after annealing at 1323, 1373 and 1423 K are shown in Fig. 4 (a), (b) and (c), respectively. With increasing annealing temperatures, $|\Delta S_M|$ increases and T_C decreases, which agrees with the previous report on the effect of annealing temperature for $MnFe_{0.95}P_{0.595}Si_{0.33}B_{0.075}$ alloys [14,15]. On the other hand, for increasing V substitutions, $|\Delta S_M|$ decreases and T_C decreases. The alloy with $x = 0.02$ annealed at 1373 K even has a larger $|\Delta S_M|$ value (18.4 $Jkg^{-1}K^{-1}$) than that with $x = 0.00$ (17.2 $Jkg^{-1}K^{-1}$) under an external field of 1 T. For a field change of 0–2 T, these two samples have equal values of $|\Delta S_M|$. This indicates that the alloy with 0.02 at% has better low-field (1 T) performance.

Since 1 T is the magnetic field applied in current heat pump prototypes with low-cost NdFeB permanent magnets, it is very significant to have high performance under this field. The current alloys with $x = 0.00$ annealed at 1323 K ($|\Delta S_M| = 8.2$ J/(kgK) at 282 K for a field change of 0–1 T with $\Delta T_{hys} = 2.1$ K) is comparable to the boron doping alloys such as the $MnFe_{0.95}P_{0.595}Si_{0.33}B_{0.075}$ alloys annealed at 1323 K ($|\Delta S_M| = 6.2$ J/(kgK) [15] at 285 K for a field change of 0–1 T) and the $MnFe_{0.95}P_{0.593}Si_{0.33}B_{0.077}$ alloys annealed at 1373 K [9] ($|\Delta S_M| = 9.8$ J/(kg·K) at 281 K with $\Delta T_{hys} = 1.6$ K). These results suggest that both a decreasing annealing temperature and an increasing V substitution can tune the strong first-order magnetic transition to the boundary between the first-order to second-order magnetic transition in the $Mn_{1.2}Fe_{0.75}P_{0.5}Si_{0.5}$ alloys. Fig. 5 (a) illustrates the temperature dependence of the value of in-field DSC of ΔT_{ad} for several $Mn_{1.2-x}V_xFe_{0.75}P_{0.5}Si_{0.5}$ alloys annealed at 1323 K, while Fig. 5 (b) illustrates the temperature dependence of ΔT_{ad} for $Mn_{1.2-x}V_xFe_{0.75}P_{0.5}Si_{0.5}$ alloys annealed at 1373 K. The value of ΔT_{ad} is determined by using the following equation [31].

$$\Delta T_{ad} = \frac{T}{C_P(H)} \Delta S_M(H) \tag{1}$$

Where C_p(H) is the specific heat. Note that there are two peaks in the vicinity of T_C for the sample $x = 0.00$. This is in line with previous observations as two different Fe_2P-type phases with close compositions have been reported to co-exist if annealing is preferred at relative lower temperatures [14]. When x increases from 0.00 to 0.02 for the sample annealed at 1323 K, the values of

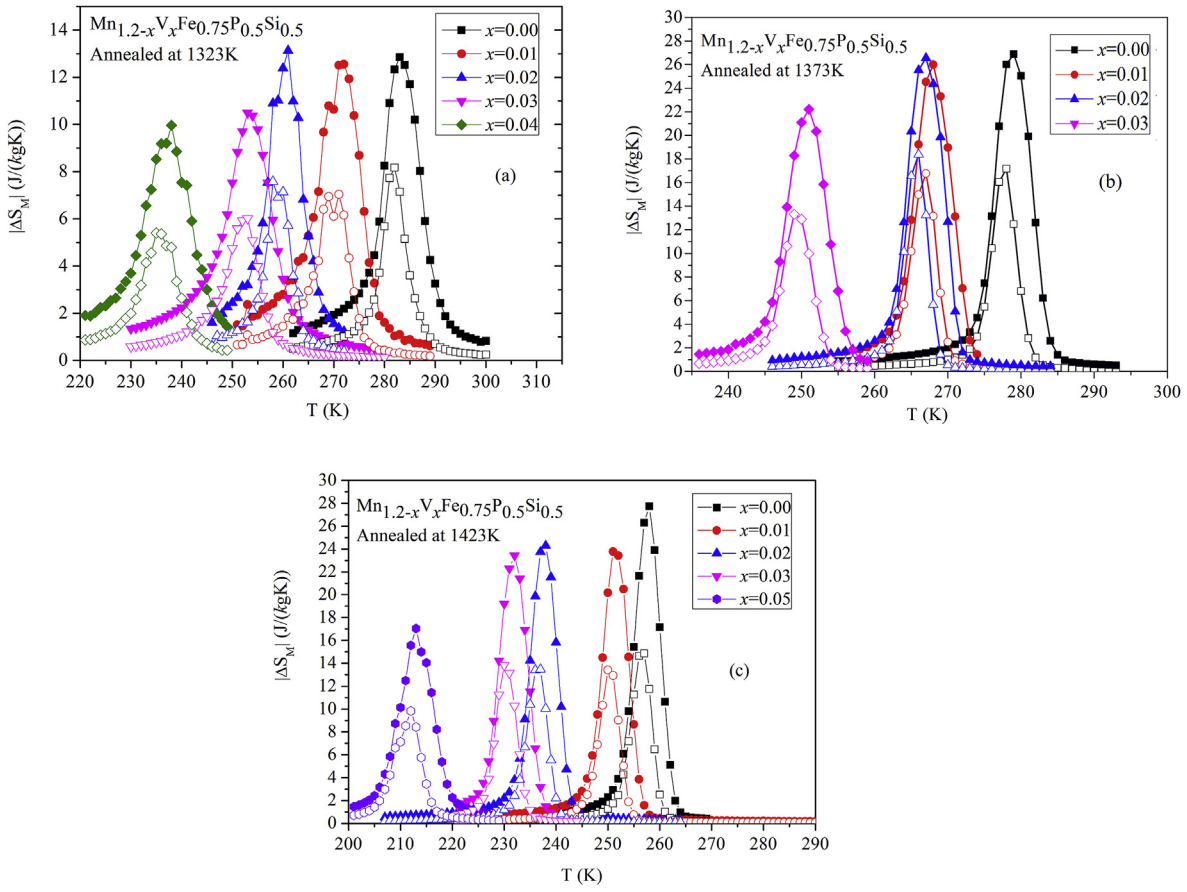

Fig. 4. (a) Temperature dependence of $|\Delta S_M|$ for a field change of 0–1 T (open symbols) and 0–2 T (solid symbols) for $Mn_{1.2-x}V_xFe_{0.75}P_{0.5}Si_{0.5}$ ($x = 0, 0.01, 0.02, 0.03, 0.04$) alloys after annealing at 1323 K; (b) Temperature dependence of $|\Delta S_M|$ for a field change of 0–1 T (open symbols) and 0–2 T (solid symbols) for $Mn_{1.2-x}V_xFe_{0.75}P_{0.5}Si_{0.5}$ ($x = 0, 0.01, 0.02, 0.03$) alloys after annealing at 1373 K; (c) Temperature dependence of $|\Delta S_M|$ for a field change of 0–1 T (open symbols) and 0–2 T (solid symbols) for $Mn_{1.2-x}V_xFe_{0.75}P_{0.5}Si_{0.5}$ ($x = 0, 0.01, 0.02, 0.03, 0.05$) alloys after annealing at 1423 K.

Table 3
Refined interatomic distances of the $Mn_{1.2}Fe_{0.75}P_{0.5}Si_{0.5}$ alloys annealed at 1323, 1373 and 1423 K and the $Mn_{1.18}V_{0.02}Fe_{0.75}P_{0.5}Si_{0.5}$ alloy annealed at 1373 K.

		$x = 0.00$(1323 K)	$x = 0.00$(1373 K)	$x = 0.00$ (1423 K)	$x = 0.02$ (1373 K)
Metal-metal distance (Å)					
Mn(3*g*)-(3*g*)	Iinterlayer	3.206(5)	3.200(7)	3.194(5)	3.198(5)
Fe/Mn(3*f*)-(3*f*)	Interlayer	2.683(1)	2.681(7)	2.663(6)	2.682(3)
Mn(3*g*)-Fe/Mn(3*f*)	x 4	2.686(8)	2.686(5)	2.691(4)	2.686(5)
Mn(3*g*)-Fe/Mn(3*f*)	Mean	2.685(6)	2.684(9)	2.682(4)	2.684(6)
Metal-nonmetallic distance (Å)					
Mn(3*g*)-P/Si	Mean	2.505(9)	2.506(3)	2.500(8)	2.505(3)
Mn(3*f*)-P/Si	Mean	2.314(1)	2.314(2)	2.321(3)	2.314(1)

ΔT_{ad} increases from 1.8 to 2.7 K and $|\Delta S_M|$ decrease from 8.2 to 7.6 $Jkg^{-1}K^{-1}$ under an external field change of 1 T. Compared to the alloy without V, a significant ΔT_{ad} of 2.7 K for a field change of 1 T and a limited hysteresis (1.8 K) are achieved in the alloy with $x = 0.02$ annealed at 1323 K, indicating that it is a promising candidate for magnetic heat-pumping.

For the sample annealed at 1373 K, the values of ΔT_{ad} increases from 3.3 to 4.8 K for an external field change of 1 T by increasing x from 0.00 to 0.02. The intermediate hysteresis in these samples is about 4.5 K. Note that it is important to distinguish the value of ΔT_{ad} from the cyclic (direct) field-induced temperature changes (ΔT_{cyclic}) in first order materials showing a large hysteresis. ΔT_{cyclic} reflects the practical working situation of the magnetic heat-pumping, while the ΔT_{ad} reflects the potential [12]. For the materials with a large hysteresis, ΔT_{ad} turns out to be much higher than ΔT_{cyclic}. Thus, it is concluded that V substitution can increase ΔT_{ad} when annealed at 1323 and 1373 K.

4. Conclusions

By decreasing the annealing temperature and increasing V substitution for Mn, it is possible to tune the strong first-order magnetic transition to the boundary between the first-order to second-order magnetic transition. Increasing the V substitution brings a decrease in the *a*-axis and an increase on the *c*-axis. As a result, T_C decreases. V has shown a preference to occupy the 3*f* site and shortens the interatomic distance. Compared to V free sample, the alloy with $x = 0.02$ has a better magnetocaloric effect in a low magnetic field change of 1 T when annealing at 1323 and 1373 K. The competitive low-field performance promotes the application

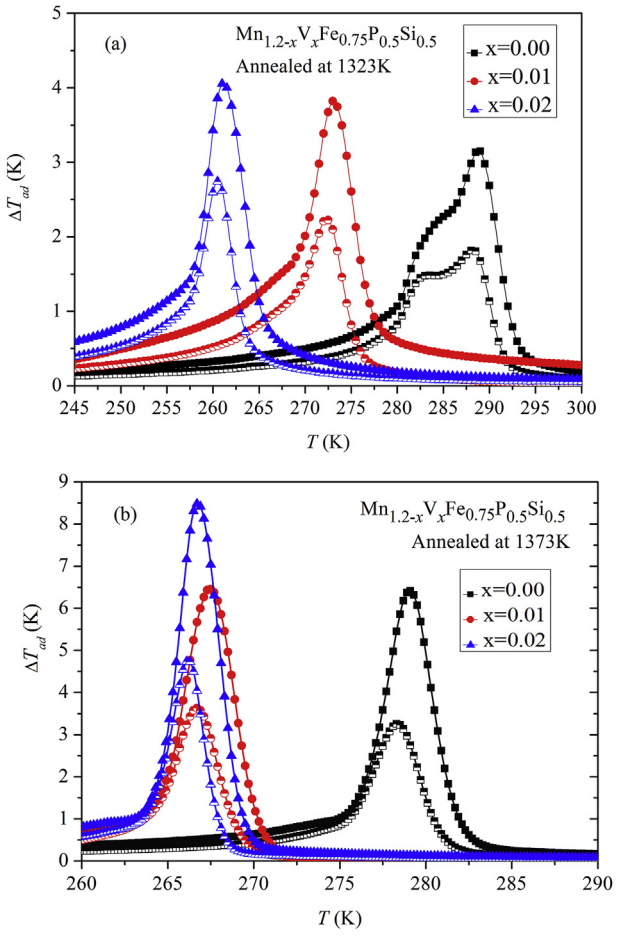

Fig. 5. (a) Temperature dependence of ΔT_{ad} for $Mn_{1.2-x}V_xFe_{0.75}P_{0.5}Si_{0.5}$ ($x = 0.00$, 0.01, 0.02) alloys annealed at 1323 K; (b) Temperature dependence of ΔT_{ad} for $Mn_{1.2-x}V_xFe_{0.75}P_{0.5}Si_{0.5}$ ($x = 0.00$, 0.01, 0.02) alloys annealed at 1373 K. The solid, half-solid and open symbols represent the applied field of 1.5 and 1.0 T, respectively.

of low-cost NdFeB permanent magnets. A larger temperature change ΔT_{ad} of 2.7 K and a low hysteresis of 1.8 K are achieved by optimizing the alloy with $x = 0.02$ annealed at 1323 K, which is comparable to the $MnFe_{0.95}P_{0.595}Si_{0.33}B_{0.075}$ alloy. $Mn_{1.2-x}V_xFe_{0.75}P_{0.5}Si_{0.5}$ alloys can therefore become a promising material for magnetic heat-pumping near room temperature.

Acknowledgements

The authors acknowledge Anton Lefering, Kees Goubitz, and Bert Zwart for their technical assistance and Dr. Yibole and Dr. Maurits Boeije for discussion. This work has been financially supported by the Dutch national research organization NWO TTW. This work is also supported by Guangdong Provincial Science and Technology Program (Grant No. 2015A050502015), the Guangzhou Municipal Science and Technology Program (No. 201707010056), the Natural Science Foundation of Guangdong Province (2016A030313494, 2018A030313615, 2018A030310406).. The author thanks the Guangzhou Ethics Project for finance support.

References

[1] E. Brück, O. Tegus, D.T.C. Thanh, K.H.J. Buschow, J. Magn. Magn. Mater. 310 (2007) 2793–2799.
[2] V.K. Pecharsky, K.A. Gschneidner, Phys. Rev. Lett. 23 (1997) 4494–4497.
[3] F.X. Hu, B.G. Shen, J.R. Sun, Z.H. Cheng, Appl. Phys. Lett. 23 (2001) 3675–3677.
[4] S. Fujieda, A. Fujita, K. Fukamichi, Appl. Phys. Lett. 81 (2002) 1276–1278.
[5] J. Liu, M. Krautz, K. Skokov, T.G. Woodcock, O. Gutfleisch, Acta Mater. 9 (2011) 3602–3611.
[6] N.H. Dung, Z.Q. Ou, L. Caron, L. Zhang, D.T. Cam Thanh, K.H.J. Buschow, E. Brück, Advanced Energy Materials 6 (2011) 1215–1219.
[7] N.H. Dung, L. Zhang, Z.Q. Ou, K.H.J. Buschow, Scripta Mater. 12 (2012) 975–978.
[8] F. Guillou, G. Porca`ri, H. Yibole, N.H. van Dijk, E. Brück, Adv. Mater. 17 (2014) 2671–2675.
[9] N. Trung, L. Zhang, L. Caron, K. Buschow, E. Brück, Appl. Phys. Lett. 96 (2010) 172504.
[10] J. Liu, T. Gottschall, K.P. Skokov, J.D. Moore, O. Gutfleisch, Nat. Mater. 11 (2012) 620.
[11] F. Guillou, H. Yibole, G. Porcari, L. Zhang, N.H. van Dijk, E. Brück, J. Appl. Phys. 116 (2014), 063903.
[12] Z.Q. Ou, N.H. Dung, L. Zhang, L. Caron, E. Torun, N.H. van Dijk, O. Tegus, E. Brück, J. Alloy. Comp. 730 (2018) 392.
[13] J.W. Lai, Z.G. Zheng, B.W. Huang, H.Y. Yu, Z.G. Qiu, Y.L. Mao, S. Zhang, F.M. Xiao, D.C. Zeng, K. Goubitz, E. Brück, J. Alloy. Comp. 735 (2018) 2567.
[14] N.V. Thang, H. Yibole, N.H. van Dijk, E. Brück, J. Alloy. Comp. 699 (2017) 633–637.
[15] N.H. Dung, L. Zhang, Z.Q. Ou, E. Brück, Appl. Phys. Lett. 99 (9) (2011), 092511.
[16] L. van Eijck, L.D. Cussen, G.J. Sykora, E.M. Schooneveld, N.J. Rhodes, A. van Well, C. Pappas, J. Appl. Crystallogr. 49 (2016) 1.
[17] H.M. Rietveld, J. Appl. Crystallogr. 2 (2) (1969) 65–71.
[18] J. Rodríguez-Carvajal, in: Satellite Meeting on Powder Diffraction of the XV IUCr Congress, vol. 127, 1990.
[19] H.P. Myers, Introductory Solid State Physics, second ed., Taylor & Francis, London, 1997, ISBN 0748406603.
[20] V. Provenzano, A.J. Shapiro, R.D. Shull, Nature 429 (2004) 853–857.
[21] D.T. Cam Thanh, E. Brück, N.T. Trung, J.C.P. Klaasse, K.H.J. Buschow, Z.Q. Ou, O. Tegus, L. Caron, J. Appl. Phys. 103 (7) (2008), 07B318.
[22] N.H. Dung, Z.Q. Ou, L. Caron, L. Zhang, D.T.C. Thanh, G.A. de Wijs, R.A. de Groot, K.H.J. Buschow, E. Brück, Adv. Energy Mater. 1 (2011) 1215.
[23] O. Gutfleisch, T. Gottschall, M. Fries, D. Benke, I. Radulov, K.P. Skokov, H. Wende, M. Gruner, M. Acet, P. Entel, M. Farle, Phil. Trans. Ser. A Math. Phys. Eng. Sci. (2016) 374.
[24] N.H. Dung, L. Zhang, Z.Q. Ou, L. Zhao, L. van Eijck, A.M. Mulders, M. Avdeev, E. Suard, N.H. van Dijk, E. Brück, Phys. Rev. B 86 (2012), 045134.
[25] M.F.J. Boeije, P. Roy, F. Guillou, H. Yibole, X.F. Miao, L. Caron, D. Banerjee, N.H. van Dijk, R.A. de Groot, E. Brück, Chem. Mater. 28 (14) (2016) 4901–4905.
[26] X.B. Liu, Z. Altounian, J. Appl. Phys. 105 (7) (2009), 07A902.
[27] X.F. Miao, S.Y. Hu, F. Xu, E. Brück, Rare Met. 37 (2018) 723.
[28] X.F. Miao, Y. Mitsui, A. Iulian Dugulan, L. Caron, N.V. Thang, P. Manue, K. Koyama, K. Takahashi, N.H. van Dijk, E. Brück, Phys. Rev. B 94 (2016), 094426.
[29] K.A. Gschneidner Jr., V.K. Pecharsky, A.O. Tsokol, Rep. Prog. Phys. 68 (2005) 1479.
[30] J.S. Blázquez, V. Franco, A. Conde, T. Gottschall, K.P. Skokov, O. Gutfleisch, Appl. Phys. Lett. 109 (2016) 122410.
[31] M. Földeàki, R. Chahine, T.K. Bose, J. Appl. Phys. 77 (1995) 3528.